SSRG International Journal of Electrical and Electronics Engineering
ISSN: 2348-8379/ https://doi.org/10.14445/23488379/IJEEE-V13I5P113

Volume 13 Issue 5, 161-171, May 2026

Original Article

Fuzzy MPPT Enabled PV Integration to Grid Through a GFL Asymmetrical 31-Level Inverter Without an LC Filter

Rampalli Jagan[1], Bhaskar Kanna[2]

[1,2]*Department of Electrical and Electronics Engineering, JNTUH University College of Engineering Science and Technology, Kukatpally, Hyderabad, India.*

[1]*Corresponding Author : jagan.gnit@gmail.com*

Received: 21 February 2026 Revised: 19 March 2026 Accepted: 18 April 2026 Published: 30 May 2026

Abstract *- Integration of renewable sources into the grid is a critical task, as the renewable sources generate power mostly in DC. The grid to which it is connected is a three-phase AC grid, where the renewable source needs to be synchronized to the grid voltage magnitude and frequency. In order to achieve this, a GFL asymmetrical 31-level inverter is employed. The inverter is connected to multiple Fuzzy MPPT-based PV units with asymmetrical voltage levels for the generation of multi-level voltages. Each phase comprises four PV units, which generate voltage levels at Vdc, 2Vdc, 4Vdc, and 8Vdc. The Fuzzy MPPT-enabled PV-integrated asymmetrical 31-level three-phase inverter is connected to the grid without an LC filter. This reduces the power losses and the cost of the converter, as a high-rated LC filter module needs to be integrated. The inverter needs a feedback signal for synchronizing with the grid, which is generated by the GFL controller. A simulation analysis is carried out on the proposed PV-grid connected system, presenting all the parameters of the system. The THD of the PCC voltages and inverter currents is maintained as per the IEEE standards (below 5%) even without the LC filter. The power loss is ensured to be maintained at a low level, increasing the efficiency of the system. The complete analysis is done by using the MATLAB Simulink tool with graphs of the measured parameters plotted with time as reference.*

Keywords *- GFL (Grid Following), MPPT (Maximum Power Point Tracking), PV (Photo Voltaic), THD (Total Harmonic Distortion), PCC (Point of Common Coupling), MATLAB.*

1. Introduction

The air quality around us is deteriorating day by day, leading to chronic lung diseases and a reduction in life expectancy. This is caused by the generation of electricity using fossil fuels and the utilization of internal combustion engine vehicles. The emissions caused by burning fossil fuels for the generation of electrical power contributes 58% of air pollution around us. However, in view of the climate, power generation by renewable energy sources will reduce gas emissions and pollution compared to fossil fuel systems, but initially needs a high capital cost. The pollution from the coal power plants will impact public health; in order to reduce the air pollution caused by the fossil fuel combustion power generation, these sources need to be replaced by renewable sources. The renewable sources are natural sources like wind, solar radiation, biogas, tidal waves, etc., for generating electrical power and to reduce CO_2 emissions [2]. There are many renewable sources available in today's technical advancements. The high rating renewable source is considered to be a wind energy conversion system that can generate more power from the wind flow. The larger wind turbine will produce the power with a lower impact on weather pollution, and wind conversion is a more sustainable option to produce the power. However, the high installation cost and the specific location for placement of the wind farm make it more complex to operate. The solar plants are considered to be a more flexible option as the PV panels can be placed in any location, and the installation cost is also much lower compared to wind farms, but both are sustainable alternatives for power generation and will reduce greenhouse gas emissions compared to fossil fuels [3].

The PV panels can also be installed in domestic (residential) areas for local power generation, providing power to a single house or a group of small houses. In the conventional technique, a single boost converter is connected for maximum power extraction from all panels, and a single inverter is used for converting DC to three-phase AC. As the inverter is a conventional two-level six-switch inverter, the output voltage is PWM AC. In order to convert the PWM AC to Sine AC, an LC filter is used, which is connected between the inverter and the grid [5].

This increases the losses and cost of the PV module. There is also a risk of failure as the complete system depends on a single boost converter. With an improper design of the LC filter, more harmonics are injected into the grid by the inverter. In order to challenge these issues in existing models, a Fuzzy MPPT-enabled PV unit with a three-phase Asymmetrical 31-level inverter is introduced to avoid the LC filter. This inverter generates an AC voltage almost similar to a sinusoidal wave, which can be integrated directly into the grid without the LC filter. The PV unit comprises four sets of PV panels, boost converters, and a Fuzzy MPPT, generating power at different voltage levels.

These voltage levels are set to Vdc, 2Vdc, 4Vdc, and 8Vdc, which help to create a 31-level AC voltage at the inverter output [7].

Three sets of PV units and asymmetrical inverters are modelled with an individual controller representing a three-phase inverter system. The neutrals of each single-phase inverter are grounded, and the phase terminals are connected directly to the grid [8]. The outline of the Fuzzy MPPT enabled PV connected three-phase Asymmetrical 31-level inverter with grid interconnection through transformer is presented in Figure 1.

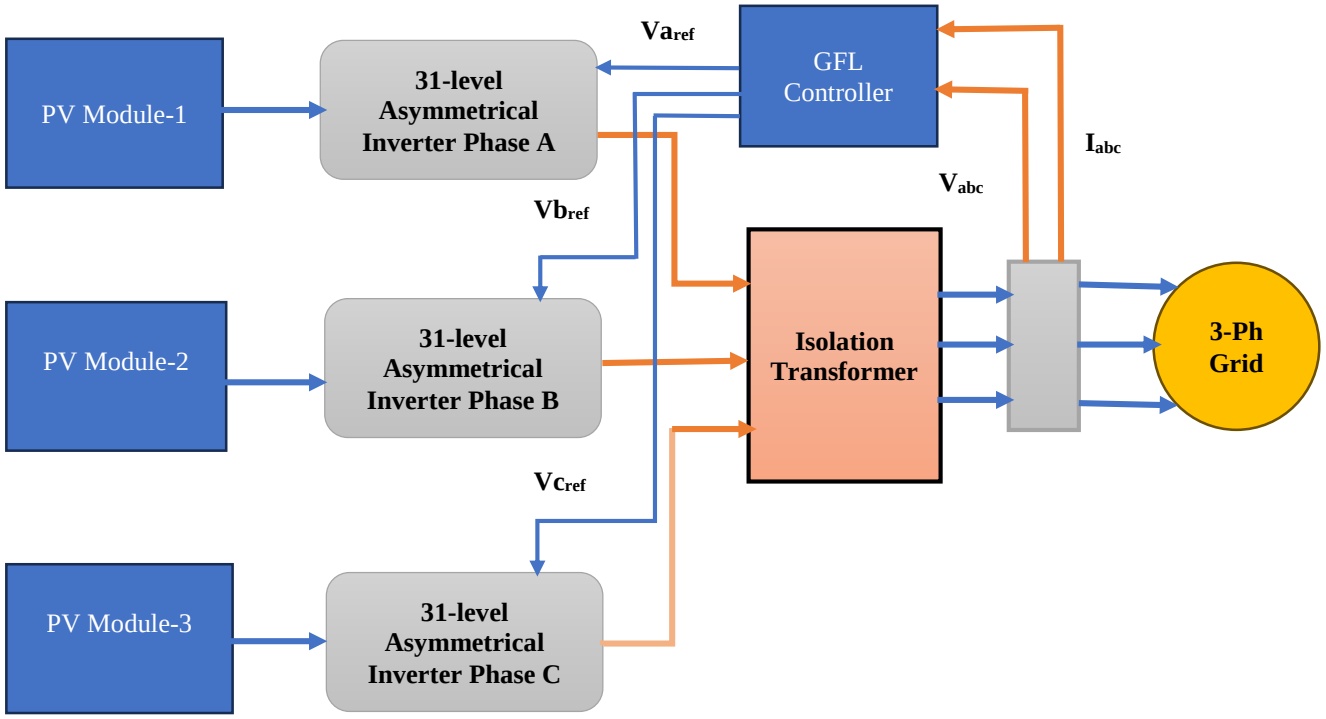

Fig. 1 Structure of Grid-connected PV integrated Asymmetrical 31-level inverter

Each PV module is connected to an individual 31-level Asymmetrical inverter, which receives a feedback signal (Vref) from the GFL controller [9]. The GFL controller needs three-phase voltages and currents feedback from the secondary side of the isolation transformer, as the inverter needs to be synchronized to the grid voltages. The GFL controller has droop control loops and current control loops [10]. The controllers estimate the reference sinusoidal signals (Vabcref) for the Asymmetrical 31-level inverter switching module. As per the reference signals, the switching takes place, creating a grid-synchronized 31-level AC voltage. The importance of this work is to develop the model without an LC filter while maintaining THD within standard limits, as discussed in the subsequent sections.

This research paper is organized with Section 1 introducing the proposed Fuzzy MPPT-enabled PV-connected three-phase Asymmetrical 31-level inverter internal structure and modules. The following section 2 is a literature review, and section 3 gives the configuration of the PV module and inverter design with switching states. Section 4 includes the GFL controller design and the mathematical expressions used for modelling the control system. The simulation modelling and analysis of the proposed system are presented in Section 5, illustrating all the parameter measurement graphs proving the vitality of the system. Section 6 is the conclusion to the paper, which validates the results generated by the simulation analysis of the proposed system, followed by references cited.

2. Literature Review

A two-level inverter with a filter is used in the conventional grid-connected PV systems to reduce the harmonics, and these LC filters will improve the quality of the output power, and also will give the losses, increased cost, size

of the equipment, and design complexity [3]. LC filters are integrated between the grid and inverters with a linear quadratic regulator to ensure zero tracking error, but this increases the size and complexity of the system [4]. Zhang et al. (2025) introduced a grid-connected PV system LCL filter with passive damping optimisation to reduce the harmonics and increase the stability of the system using a two-level voltage source inverter.

But with the advantage of reducing the harmonics, the system suffers from power losses, thermal challenges, and complex control strategies, which limit the efficiency [5]. Hamidi et al. (2021) proposed a 31-level MLDCL inverter with the P&O MPPT method for standalone applications rather than grid integration [6].

Geng et al. proposed to improve the inverter performance for both weak and strong grid conditions with a complex control architecture and the inclusion of an LC filter, which increases hardware complexity due to a hybrid PLL-droop architecture and control loops. This Paper mainly discusses the hybrid GFL and GFM with a normal inverter with an LC filter [17]. Most topologies depend upon the filters to eliminate the harmonics, and there is limited research on filterless grid integration using multilevel inverters. However, multi-level inverters offer an improved waveform with fewer harmonics. Along with this, conventional MPPT methods will give a slower tracking response under dynamic irradiance conditions. Hence, there is a clear research gap in the grid-connected PV system with intelligent MPPT control and high-level asymmetrical multi-level inverter topology to maintain grid synchronization and harmonics within standard limits.

Based on these observations, this research work proposes Fuzzy MPPT Enabled PV Integration to Grid Through a GFL Asymmetrical 31-Level Inverter Without an LC Filter to reduce the harmonics, maintaining THD in standard limits, increasing the efficiency by reducing the losses, and improve the tracking performance.

3. PV Module and Inverter Configuration

As presented in the previous section, each PV module comprises four PV units with an individual boost converter connected to a set of PV panels. Each PV set comprises multiple series and parallel-connected panels generating different DC voltage levels.

The solar radiation-dependent voltages of the PV panels are boosted and stabilized by the boost converter operated by the Fuzzy MPPT voltage regulator controller [11]. The flow chart of the Fuzzy MPPT algorithm for the boost converter switching pulse duty ratio generation is presented in Figure 2.

The Fuzzy-based MPPT needs two measurements (Vpv and Ipv), PV panels voltage and current [12]. As per the relational comparison of the past and present values of the power (P(x) and P(x-1)) and voltage error (Verr), the specific Fuzzy MPPT is activated.

The switching of MPPT is based on the following conditions

$$MPPT\ 1 = If \begin{cases} P_{pv}(x) > P_{pv}(x-1),\ V_{err} > 0 \\ P_{pv}(x) < P_{pv}(x-1),\ V_{err} < 0 \end{cases}$$
$$MPPT\ 2 = If \begin{cases} P_{pv}(x) > P_{pv}(x-1),\ V_{err} < 0 \\ P_{pv}(x) < P_{pv}(x-1),\ V_{err} > 0 \end{cases} \quad (1)$$

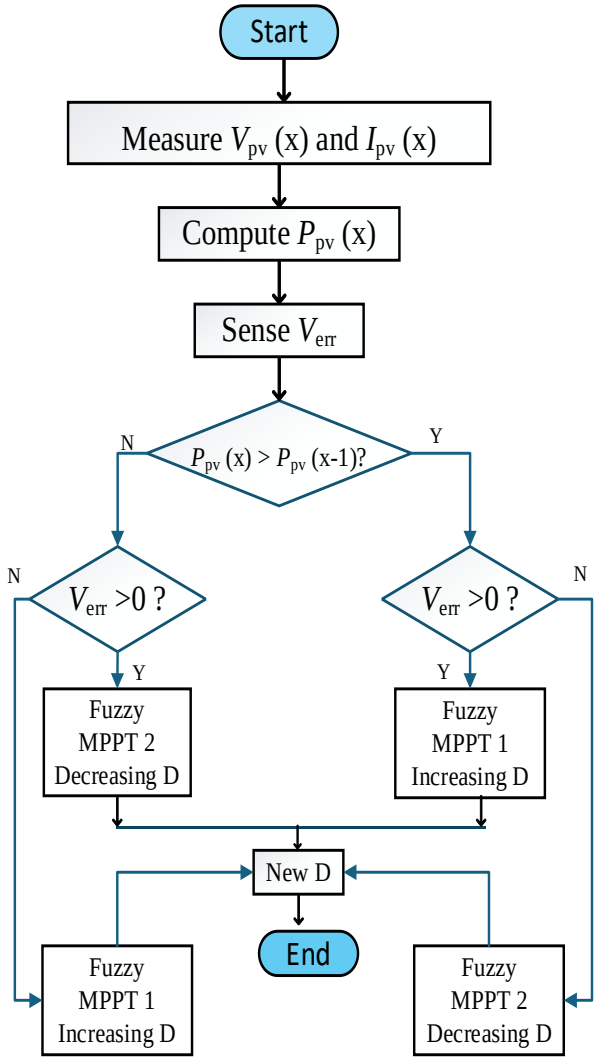

Fig. 2 Fuzzy-based MPPT algorithm flow chart

Each MPPT is included with two input variables (dP and dV) and one output variable (cD). All three variables are included with seven Membership Functions (MFs) each with a triangular type shape. The MFs are linked using rules depicting the output value region for the variation of the duty of the boost converter switch [13]. The MFs of the variables and the rule tables are presented below in Figure 3(a) 3(b) and Tables 1 and 2, respectively.

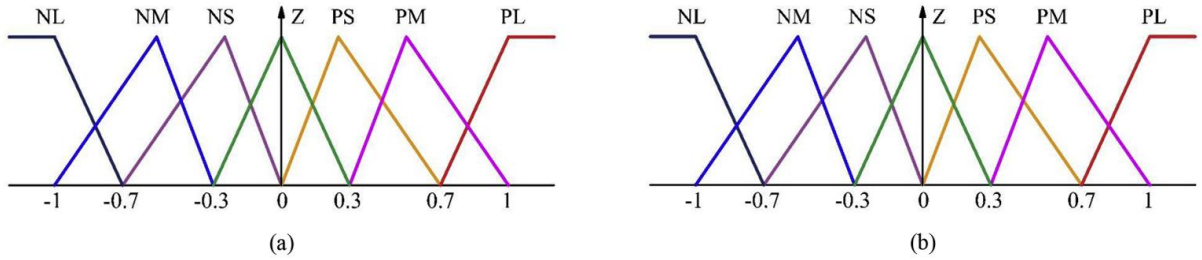

Fig. 3 Fuzzy MFs (a) dP or dV MFs, (b) cD MFs.

Table 1. MPPT 1 rule-based

cD		dP						
		NL	**NM**	**NS**	**Z**	**PS**	**PM**	**PL**
dV	**NL**	NL	NL	NM	Z	PM	PL	PL
	NM	NL	NM	NM	Z	PM	PM	PL
	NS	NL	NM	NS	Z	PS	PM	PL
	Z	Z	Z	Z	Z	Z	Z	Z
	PS	PS	PS	PS	Z	NS	NM	NL
	PM	PM	PM	PS	Z	NS	NM	NL
	PL	PL	PL	PM	Z	NM	NL	NL

Table 2. MPPT 2 rule-based

cD		dP						
		NL	**NM**	**NS**	**Z**	**PS**	**PM**	**PL**
dV	**NL**	PL	PL	PM	Z	NM	NL	NL
	NM	PL	PM	PM	Z	NM	NM	NL
	NS	PL	PM	PS	Z	NS	NM	NL
	Z	Z	Z	Z	Z	Z	Z	Z
	PS	NL	NM	NS	Z	PS	PS	PS
	PM	NL	NM	NS	Z	PS	PM	PM
	PL	NL	NL	NM	Z	PM	PL	PL

Each PV unit with a boost converter and Fuzzy MPPT is connected to the Asymmetrical 31-level inverter as presented in Figure 4.

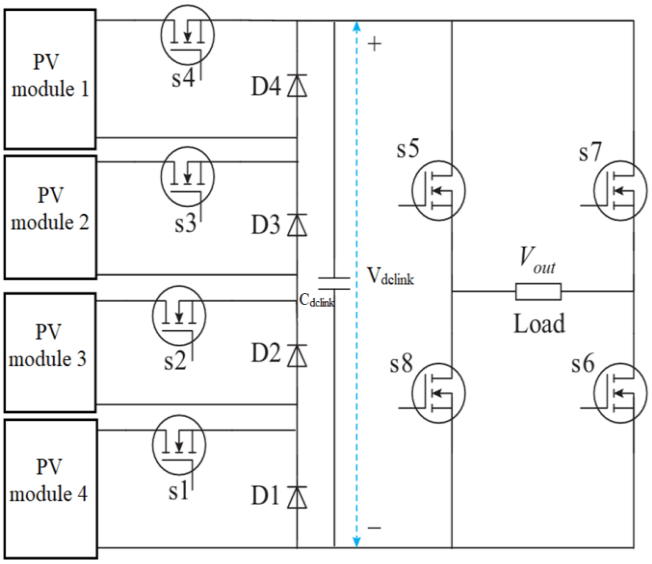

Fig. 4 PV modules connected to an asymmetrical 31-level inverter

Each phase of the complete system comprises Figure 4 topology in which the switches S5 – S8 only change the direction of the voltage from positive to negative [14]. The switches S5 and S6 turn ON to create positive voltage, and S7 and S8 turn ON to create negative voltage. The positive 15-voltage levels or the negative 15-voltage levels are created by switches S1-S4 [15]. The 15 voltage levels with the switching pattern can be observed in Table 3.

Table 3. Voltage level switching

S1	S2	S3	S4	Voltage level
0	0	0	0	0
1	0	0	0	$1*V_{dclink}$
0	1	0	0	$2*V_{dclink}$
1	1	0	0	$3*V_{dclink}$
0	0	1	0	$4*V_{dclink}$
1	0	1	0	$5*V_{dclink}$
0	1	1	0	$6*V_{dclink}$
1	1	1	0	$7*V_{dclink}$
0	0	0	1	$8*V_{dclink}$
1	0	0	1	$9*V_{dclink}$
0	1	0	1	$10*V_{dclink}$
1	1	0	1	$11*V_{dclink}$
0	0	1	1	$12*V_{dclink}$
1	0	1	1	$13*V_{dclink}$
0	1	1	1	$14*V_{dclink}$
1	1	1	1	$15*V_{dclink}$

The positive 15-voltage levels and negative 15-voltage levels, including the "0" voltage level, contribute to 31 levels created on the inverter output terminals [16]. The three sets of the Fuzzy base MPPT PV modules connected to Asymmetrical 31-level inverters create three-phase voltages. The reference voltage signals for the generation of the switching sequence are generated by the GFL controller.

4. Inverter Control Design

The 31-level asymmetrical inverter needs per-unit-based reference Sinusoidal signals for the generation of switching pulses for the inverter switches. The magnitude and phase angle of the reference sinusoidal signals are controlled by the GFL control module [17, 18]. The GFL comprises droop control with active and reactive power feedback generated by measurement of three-phase voltages and currents at the PCC [19].

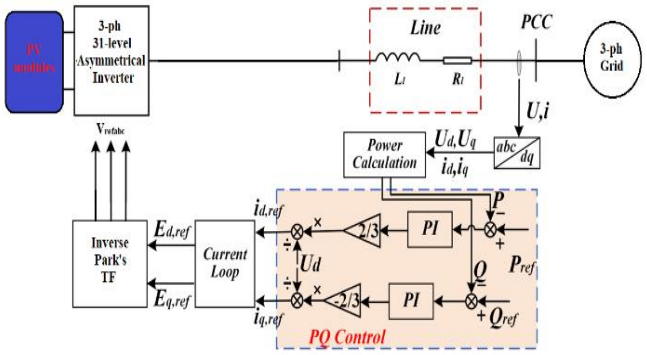

Fig. 5 GFL control structure

The complete structure of the GFL control module is presented in Figure 5.

The instantaneous active and reactive powers of the inverter output are calculated using dq components of the voltages and currents, which are achieved by Park's transformation, given as

$$\begin{bmatrix} f_d \\ f_q \end{bmatrix} = \begin{bmatrix} Sin\ wt & -Cos(wt) & 0 \\ Cos\ wt & Sin(wt) & 0 \end{bmatrix} \begin{bmatrix} f_a \\ f_b \\ f_c \end{bmatrix} \quad (1)$$

Here, variable $'f'$ can be three-phase voltages and currents ('U' or 'i') which are measured at the PCC of the test system. $'wt'$ is the phase angle of phase A of grid voltage, which is determined by PLL (phase locked loop) [20]. From the dq components of the voltage and current, the active and reactive powers (P&Q) are calculated as

$$P = \frac{3}{2}(U_d I_d + U_q I_q) \quad (2)$$

$$Q = \frac{3}{2}(U_q I_d - U_d I_q) \quad (3)$$

The reference current signals ($i_{d,\ ref,}$ and $i_{q,\ ref}$) for the generation of the current loop are expressed as

$$i_{d,ref} = \frac{1}{U_d}\left(\frac{2}{3}\left(\left(P_{ref} - P\right)\left(k_{pp} + \frac{k_{ip}}{s}\right)\right)\right) \quad (4)$$

$$i_{q,ref} = \frac{1}{U_d}\left(-\frac{2}{3}\left(\left(Q_{ref} - Q\right)\left(k_{pq} + \frac{k_{iq}}{s}\right)\right)\right) \quad (5)$$

Here, $k_{pp,q}$ and $k_{ip,q}$ are the proportional and integral gains of the PI power regulators [21]. The values of P_{ref} and Q_{ref} are set to '1' and '0' respectively, representing complete injection of active power from the inverter to the grid and no reactive power exchange between the inverter and the grid [22]. From the reference and measured current dq components, the dq reference signal components ($E_{d,\ ref}$ and $E_{q,\ ref}$) are generated as

$$E_{d,ref} = \left(i_{d,ref} - i_d\right)\left(k_{pc} + \frac{k_{ic}}{s}\right)$$

$$E_{q,ref} = \left(i_{q,ref} - i_q\right)\left(k_{pc} + \frac{k_{ic}}{s}\right) \quad (6)$$

Here, k_{pc} and k_{ic} are the proportional and integral gains of the PI current regulators [23].

The dq reference components are converted to 'abc' signals using inverse Park's transformation, expressed as

$$\begin{bmatrix} V_{refa} \\ V_{refb} \\ V_{refc} \end{bmatrix} = \begin{bmatrix} Sin\ wt & Cos\ wt \\ Sin\left(wt - \frac{2\pi}{3}\right) & Cos\left(wt - \frac{2\pi}{3}\right) \\ Sin\left(wt + \frac{2\pi}{3}\right) & Cos\left(wt + \frac{2\pi}{3}\right) \end{bmatrix} \begin{bmatrix} E_d \\ E_q \end{bmatrix} \quad (7)$$

5. Simulation Result Analysis

The simulation modelling of the presented modules is carried out in the Simulink environment of MATLAB software, utilizing blocks from the 'Electrical' block set. All the active and passive elements are considered from the 'Power Electronics' and 'Elements' block sets.

The three-phase AC source (considered as 3-ph Grid) is taken from 'Sources,' and the Photovoltaic is taken from 'Extra Sources'. All the blocks are connected as per the circuit structures mentioned in previous sections, and the block parameters are given as per Table 4.

With the parameters mentioned in Table 4 updated into the simulation blocks, the model is analysed with different operating conditions. Initially, the solar radiation is set to 1000W/m^{2,} and the model is run for a simulation time of 1sec.

Table 4. System Configuration Parameters

Name of the module	Parameters
PV panel	Model: SunPower SPR-76R-BLK-U V_{mp} = 13.5V, V_{oc} = 16.2V, I_{mp} = 5.65A, I_{sc} = 6.02A. P_{pv} = 76W Unit 1: N_p = 2; N_s = 1 Unit 2: N_p = 2; N_s = 2 Unit 3: N_p = 2; N_s = 4 Unit 4: N_p = 2; N_s = 8
Boost converter	L_b = 5mH, C_{in} = 100µF, C_{out} = 8mF, f_{sw} = 5kHz
Inverter	R_{mosfet} = 1mΩ, C_{dclink} = 1mF
Transformer	10kVA 50Hz 0.4kV/11kV
Grid	10MVA 11kV 50Hz
GFL control	K_{pp}=8.5; K_{ip}=2.3; K_{pc}=0.15; K_{ic}=0.35

The measurements for PV array characteristics, DC link voltages, AC voltages and currents, and inverter active power injection to the grid are presented.

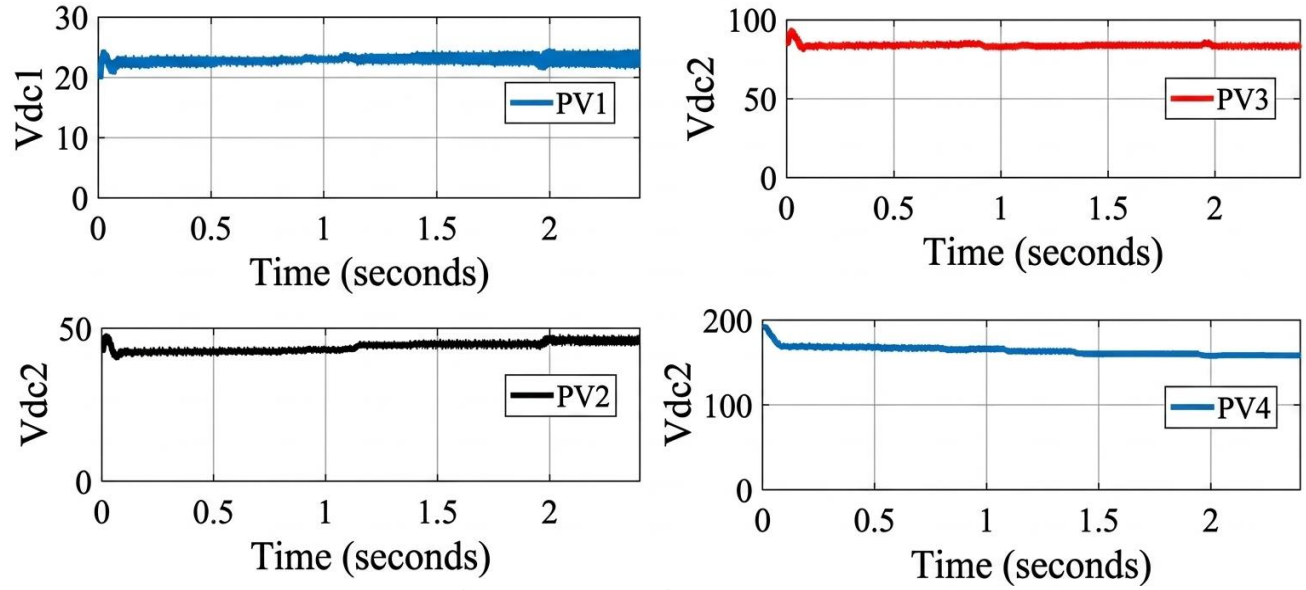

Fig. 6 DC output voltages of the boost converter of the PV module with constant solar irradiation

Figure 6 illustrates the DC output voltages of each PV unit boost converter of the four fuzzy-based PV modules. The voltage recorded is 22V, 44V, 88V, and 176V, which generate a maximum value of 330V at the output of the inverter. The Vdc is considered to be 22V to create a 330V maximum value, which is the peak value of 230Vrms of the AC voltage. The 230Vrms from each phase inverter is connected to the three-phase transformer, stepping up the voltage from 400VrmsL-L to 11kVrmsL-L. After stepping up the voltage, the secondary is connected to the three-phase grid, sharing power from the PV modules. Figure 7 shows the three-phase voltages at PCC and the injected current from the PV module into the grid.

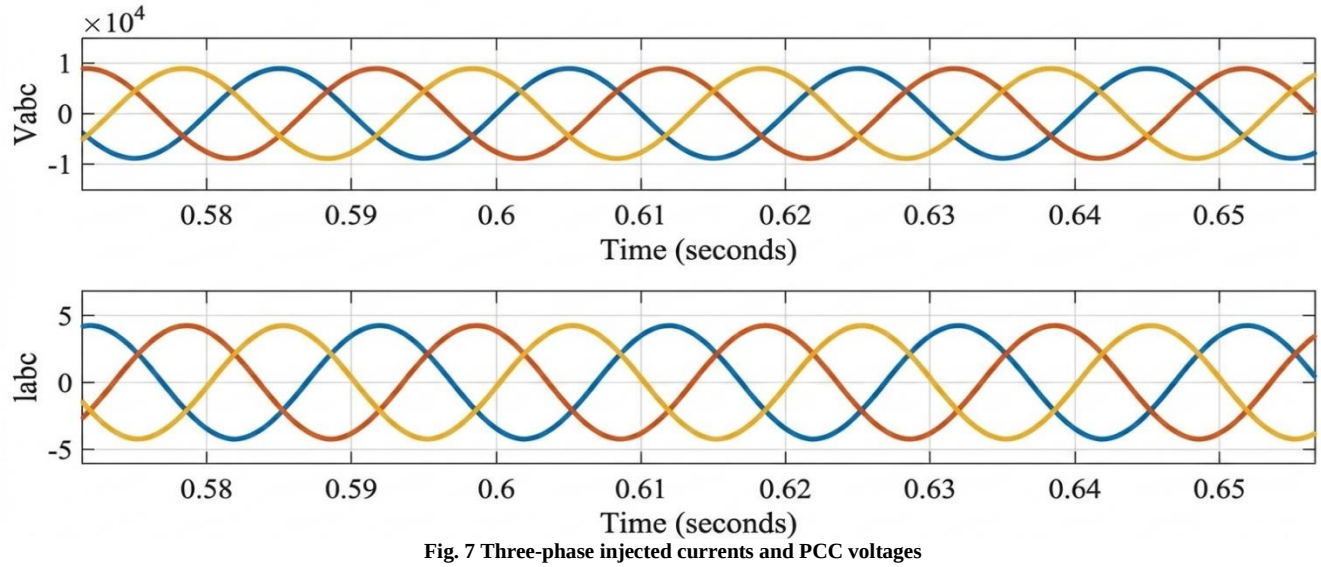

Fig. 7 Three-phase injected currents and PCC voltages

With the constant solar radiation, the power generated by the PV panels is also constant and stable. The maximum total power that can be generated by the PV panels can be estimated by the number of series and parallel panels connected in all four PV modules. As per the configuration parametric table, the maximum power generated by the PV modules is 5.6kW. As per Figure 8, the total power injected into the grid is recorded to be 5kW. The difference of 0.6kW power is the loss caused by the boost converter elements, the power electronic switches of the inverter, and the step-up transformer. The power loss and efficiency of the conventional six-switch LC filter-based inverter are shown in Figures 9(a) and 9(b), respectively. And the power loss and efficiency of the system with the asymmetrical inverter are presented in Figures 9(c) and 9(d), respectively. As per the comparison, the power loss has decreased from 1300W to 600W, and the efficiency increased from 78% to 88% when the system is updated with a 3-ph asymmetrical inverter.

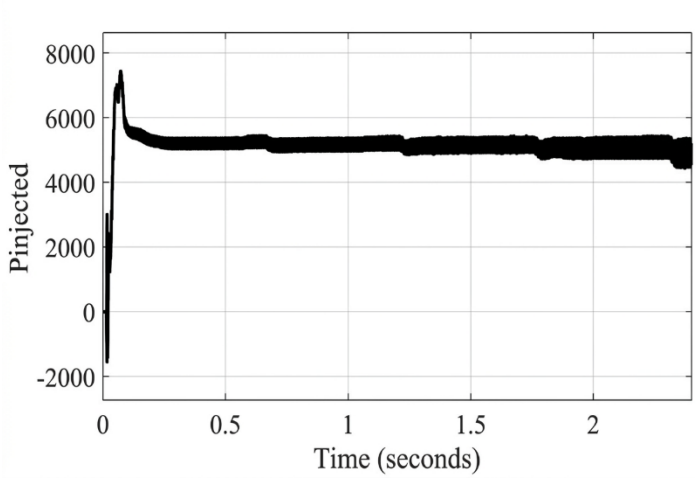

Fig. 8 Injected active power to the grid with constant solar irradiation

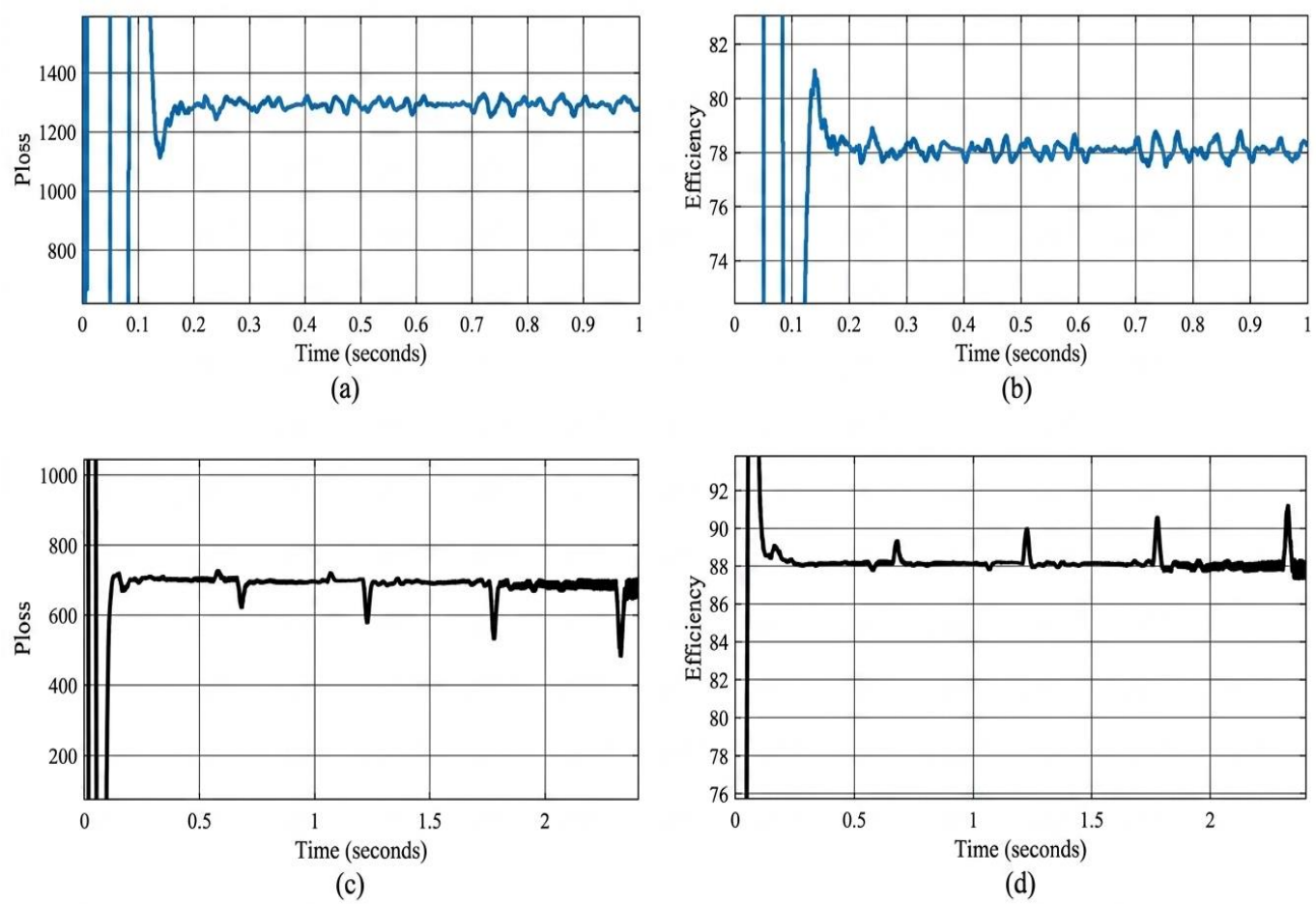

Fig. 9 (a) Total power loss of the six-switch inverter, (b) Efficiency of the six-switch conventional model, (c) Total power loss of the proposed inverter, (b) Efficiency of the proposed model.

In order to analyse the proposed system, a practical day variation solar radiation is considered with a simulation time of 2.4sec representing 24 hr scale in real time, the solar radiation starts to rise from 0.6sec representing 6 am, reaching. Peak value at 1.3sec representing 1 pm.

The radiation starts dropping from 1.3sec and drops to zero at 1.8sec, representing 6 pm. The DC voltage outputs of the PV module boost converters for the given day variation of solar radiation are illustrated in Figure 10.

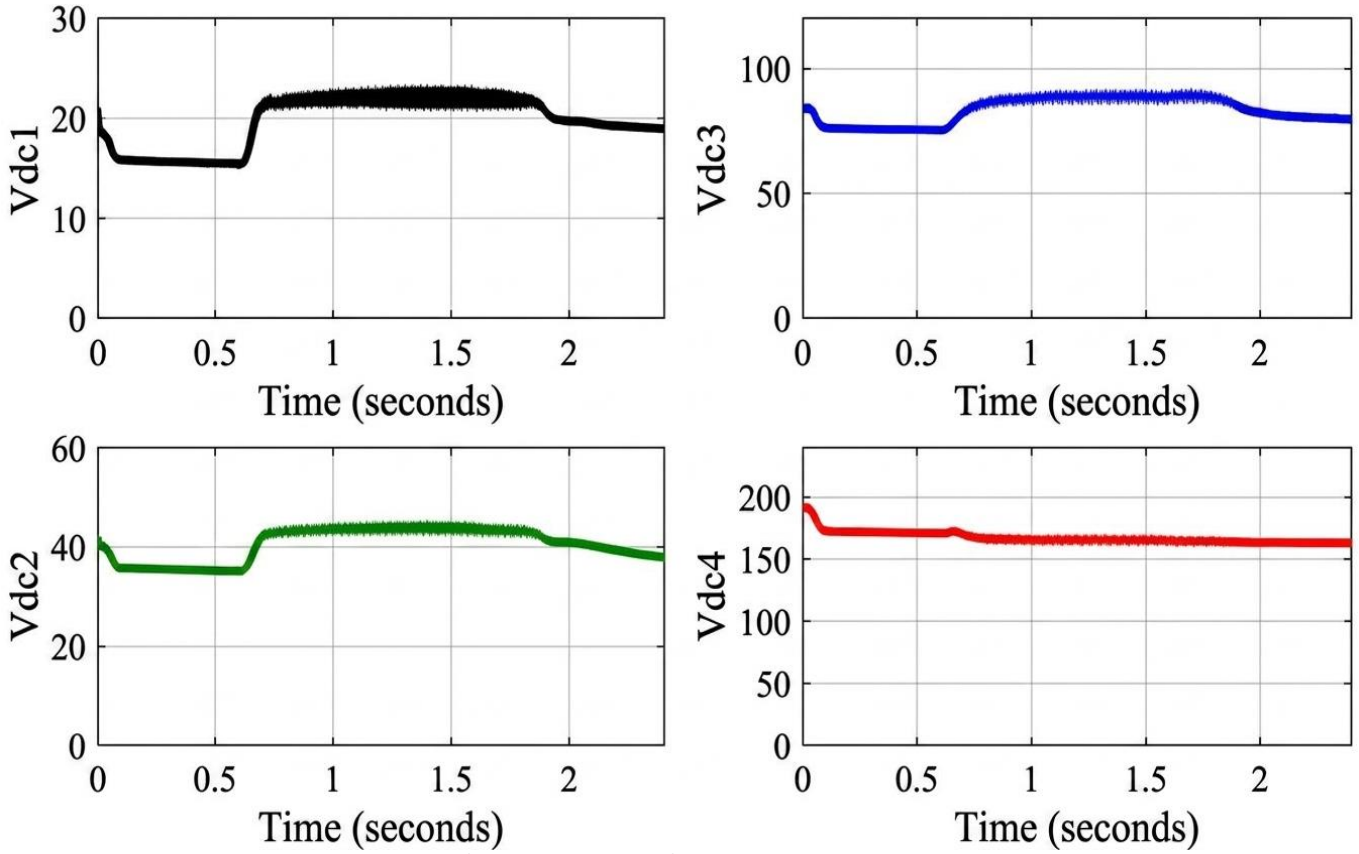

Fig. 10 DC output voltages of the boost converter of the PV module with 24hr emulation solar irradiation

As presented in Figure 10, the voltages of all the boost converters are at a lower value until 0.6sec when the solar radiation is zero.

The output voltage value rises to the required value. desired value when the solar radiation rises at 0.6sec and maintains till 1.8sec until the radiation drops to zero.

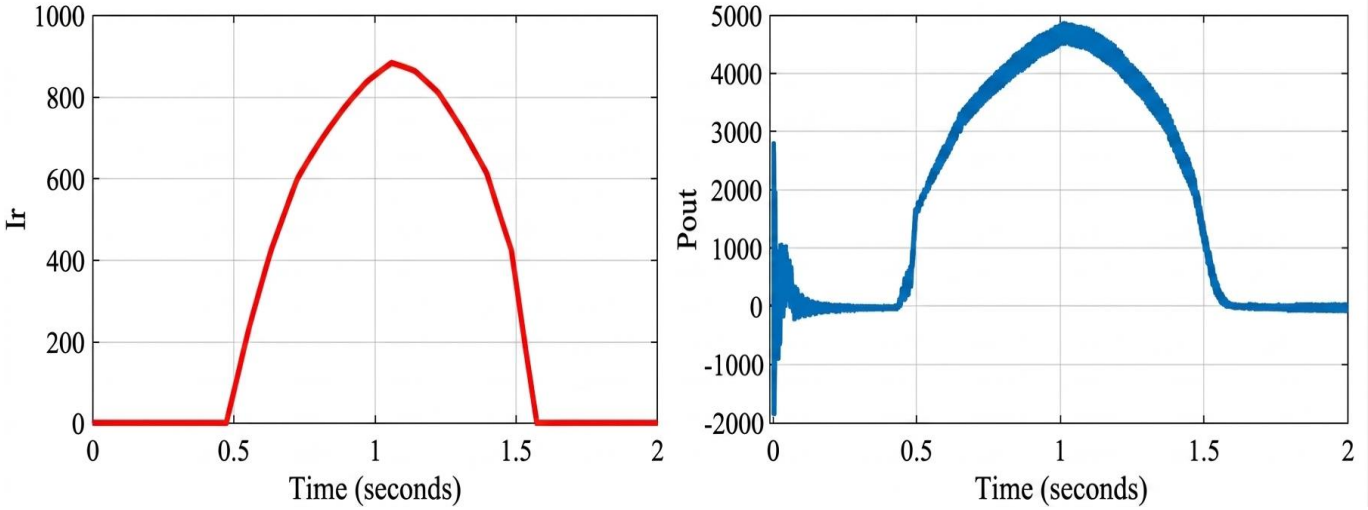

Fig. 11 (a) Solar irradiation, (b) Injected power to the grid with 24hr emulation.

As per Figure 11, the injected active power rises from zero at 0.6sec to 5kW peak till 1.3sec, further dropping to zero at 1.8sec. The active power injection replicates the solar radiation pattern emulated in a scale of 24 hours with a simulation time of 2.4sec. The power loss and the efficiency of the complete system with PV panels, boost converter and asymmetrical inverter operating in variable solar radiation is presented in figure 12(a) and 12(b) respectively.

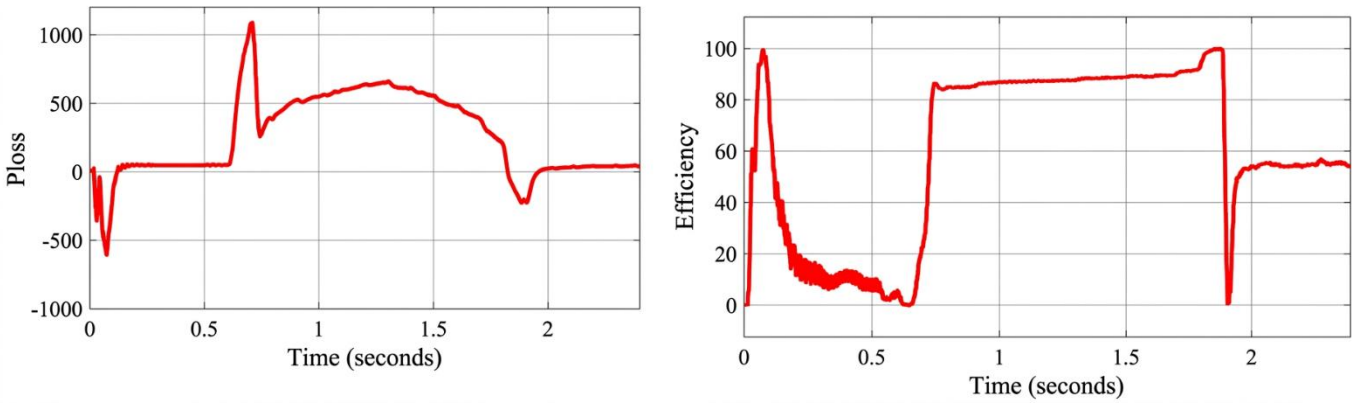

Fig. 12 (a) Power loss during variable solar radiation, (b) Efficiency during variable solar radiation.

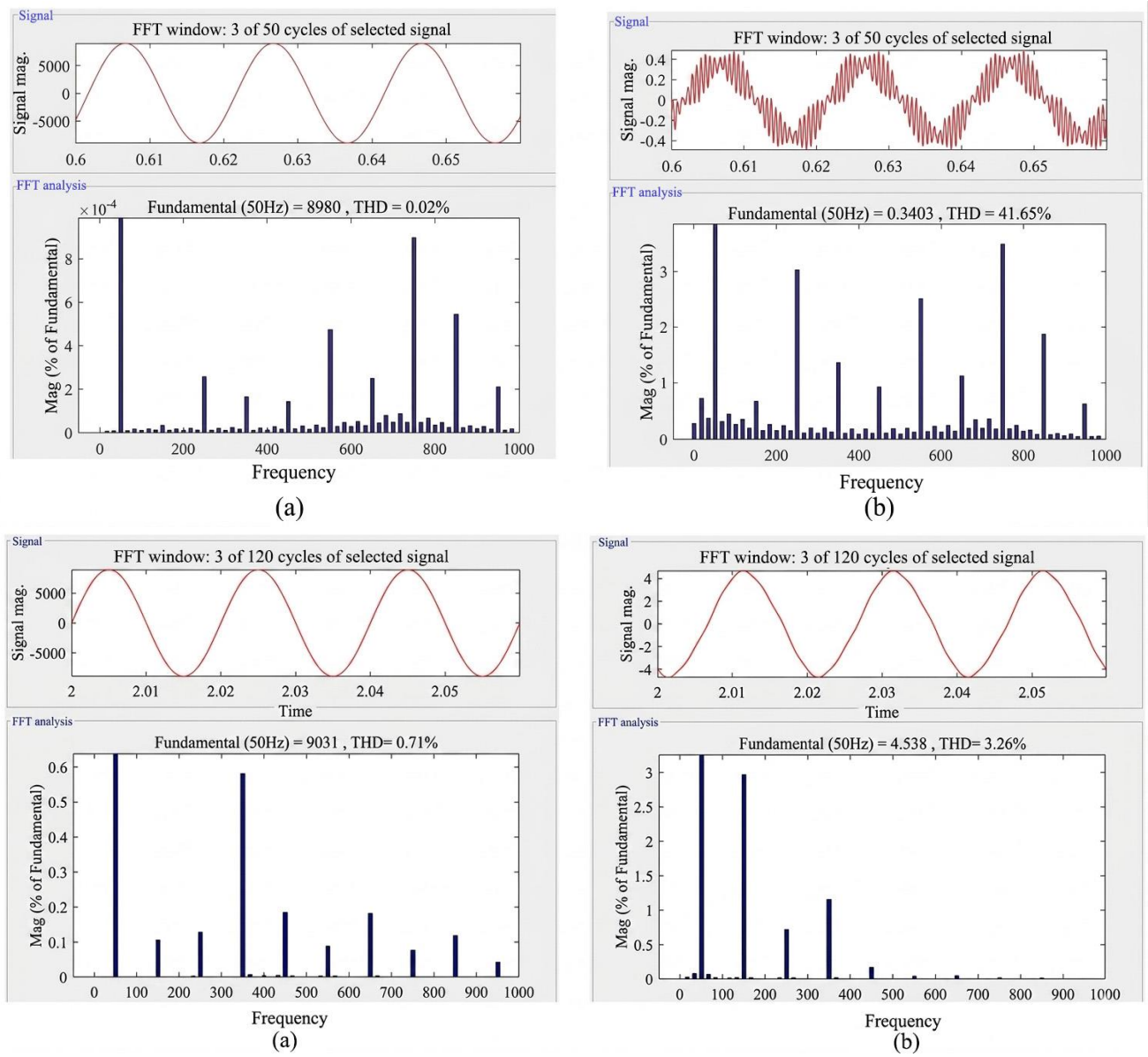

Fig. 13 THDs of the (a) Six switch inverter model PCC voltage, (b) Six switch inverter injected current, (c) Proposed converter PCC voltage, (d) Proposed inverter injected current.

The above figures 13(a) and 13(b) are the THDs of the PCC voltage and injected current from the inverter to the grid for the six-switch LC-filter based inverter. And the figures 13(c) and 13(d) are the THDs of the PCC voltage and injected current from the inverter to the grid with the proposed 3-ph asymmetrical inverter.

It can be observed that there is a significant drop in the inverter current THD from 41.65% to 3.26% when the system is updated to an asymmetrical inverter. However, there is a negligible increase in the THD of the PCC voltage, which is recorded to be 0.71%. According to the IEEE 519-2022 standards, the voltage and current THDs are maintained below 5%, and the system is operating in a stable state. A comparative analysis is presented in Table 5 between the conventional 2-level system and the proposed system.

Table 5. Comparative analysis

S. No.	Parameter	Conventional Inverter	Proposed System
1	Inverter Type	Two-level	31-level asymmetrical
2	LC Filter	Required	Not required
3	Current THD	41.65%	3.26%
4	Efficiency	78%	88%
5	Power Loss	1300 W	600 W

6. Conclusion

In this research work, the implementation of the Asymmetrical 31-level inverter with Fuzzy MPPT enabled PV modules injecting power into the grid without the LC filter is achieved using Simulink environment in MATLAB. The multiple PV units help to generate different voltage levels for creating 31 voltage levels by the asymmetrical inverter. The Asymmetrical inverter receives a reference signal from the GFL controller, which uses PCC voltage and inverter current signals for the generation of the reference signal. The GFL controller uses droop control loops, which include power and current regulators generating reference sinusoidal signals for switching of the inverter. The three-phase AC voltages generated by individual inverters are stepped up to the grid voltage, and the power is shared without an LC filter. The system efficiency is calculated to be 88% with converter losses of 0.6kW observed in the simulation analysis. The THD of the voltage and current at the secondary of the transformer is recorded to be within the standard limits. In terms of cost effectiveness, each LC filter for a lower-level multi-level inverter will be 20k – 30k INR, which would greatly affect the total cost of the inverter. With this proposed asymmetrical multi-level inverter, the LC filter is completely eliminated, with an increase in switch cost considered to be lower than the cost of the LC filter. The future work can also be done with advanced MPPT methods and by increasing the level of the inverter.

References

[1] Sarath K. Guttikunda, and Puja Jawahar, "Atmospheric Emissions and Pollution from the Coal-Fired Thermal Power Plants in India," Atmospheric Environment, vol. 92, pp. 449-460, 2014. [CrossRef] [Google Scholar] [Publisher Link]

[2] Azizullah Faizi et al., "Environmental Impacts of Natural Resources, Renewable Energy, Technological Innovation, and Globalization: Evidence from the Organization of Turkic States," *Sustainability*, vol. 16, no. 22, 2024. [CrossRef] [Google Scholar] [Publisher Link]

[3] Burcin Atilgan Turkmen, and Fatos Germirli Babuna, "Life Cycle Environmental Impacts of wind Turbines: A Path to Sustainability with Challenges," *Sustainability*, vol. 16, no. 13, 2024. [CrossRef] [Google Scholar] [Publisher Link]

[4] Said Al-Abri et al., "Optimal Tracking for PV Three-Phase Grid-Connected Inverter with LC Filter," *Franklin Open*, vol. 8, 2024. [CrossRef] [Google Scholar] [Publisher Link]

[5] Yue Zhang et al., "Optimization of Passive Damping for LCL-Filtered AC Grid-Connected PV-Storage Integrated Systems," *Electronics*, vol. 14, no. 4, 2025. [CrossRef] [Google Scholar] [Publisher Link]

[6] Muhammad Najwan Hamidi et al., "Asymmetrical Multi-Level DC-Link Inverter for PV Energy System with Perturb and Observe Based Voltage Regulator and Capacitor Compensator," *Journal of Modern Power Systems and Clean Energy*, vol. 9, no. 1, pp. 199-209, 2021. [CrossRef] [Google Scholar] [Publisher Link]

[7] Abdulhasan F. Abdulhasan, Fatimah F. Jaber, and Yousif Abdulwahab Kheerallah, "Design and Simulation of Reduced Switch 31-Level Multilevel Inverter Topology for PV Application," *Iraqi Journal for Electrical and Electronic Engineering*, vol. 21, no. 1, pp. 178-188, 2024. [CrossRef] [Google Scholar] [Publisher Link]

[8] Murugesan Manivel et al., "Performance Analysis of Thirty-One Level Multilevel Inverter for Electric Vehicle Application," *Proceedings of the Bulgarian Academy of Sciences*, vol. 77, no. 3, pp. 380-389, 2024. [CrossRef] [Google Scholar] [Publisher Link]

[9] V. Vignesh Babu et al., "Development of Grid-Forming and Grid-Following Inverter Control in Microgrid Network Ensuring Grid Stability and Frequency Response," *Electronics*, vol. 13, no. 10, 2024. [CrossRef] [Google Scholar] [Publisher Link]

[10] Anas Karaki, Ali Sharida, and Sertac Bayhan, "An Improved Predictive Control Strategy for Grid-Following Inverters during Voltage Sag," *2025 IEEE 19th International Conference on Compatibility, Power Electronics and Power Engineering (CPE-POWERENG)*, Antalya, Türkiye, pp. 1-6, 2025. [CrossRef] [Google Scholar] [Publisher Link]

[11] Mustapha Melhaoui et al., "Hybrid Fuzzy Logic Approach for Enhanced MPPT Control in PV Systems," *Scientific Reports*, vol. 15, 2025. [CrossRef] [Google Scholar] [Publisher Link]

[12] Sunkara Sunil Kumar, and K. Balakrishna, "A Novel Design and Analysis of Hybrid Fuzzy Logic MPPT Controller for Solar PV System under Partial Shading Conditions," *Scientific Reports*, vol. 14, 2024. [CrossRef] [Google Scholar] [Publisher Link]

[13] Maher G. M. Abdolrasol et al., "Fuzzy Controller-Driven Pattern Search Optimization for a DC–DC Boost Converter to Enhance Photovoltaic MPPT Performance," *Scientific Reports*, vol. 15, 2025. [CrossRef] [Google Scholar] [Publisher Link]

[14] A. Praveena, and K. Sathishkumar, "Power Quality Improvement Using a 31-Level Multilevel Inverter with Bio-Inspired Optimization Approach," *Frontiers in Energy Research*, vol. 12, 2024. [CrossRef] [Google Scholar] [Publisher Link]

[15] Taha Ahmad Hussein, Dahaman Ishak, and Mohamad Tarnini, "A Three-Phase Multilevel Inverter Synthesized with 31 Levels and Optimal Gating Angles Based on the GA and GWO to Supply a Three-Phase Induction Motor," *Energies*, vol. 17, no. 5, 2024. [CrossRef] [Google Scholar] [Publisher Link]

[16] P. V. V. Raghava Sharma, and N. Kashappa, "Design and Analysis of 31 Level Cascaded H-bridge Multilevel Inverter," International Education & Research Journal, vol. 10, no. 5, pp. 47-50, 2024. [Publisher Link]

[17] Fatih Burak, and Hulusi Karaca, "Comparative Analysis of Grid-Following (GFL) and Grid-Forming (GFM) Inverters: Control and Transition Capabilities," *Electrical Engineering and Energy*, vol. 4, no. 1, pp. 40-51, 2025. [CrossRef] [Google Scholar] [Publisher Link]

[18] Sijia Geng, and Ian A. Hiskens, "Unified Grid-Forming/Following Inverter Control," *IEEE Open Access Journal of Power and Energy*, vol. 9, pp. 489-500, 2022. [CrossRef] [Google Scholar] [Publisher Link]

[19] Sunjoh Christian Verbe et al., "Dynamic Control of Grid-Following Inverters Using DC Bus Controller and Power-Sharing Participating Factors for Improved Stability," *Energy Reports*, vol. 12, pp. 4489-4500, 2024. [CrossRef] [Google Scholar] [Publisher Link]

[20] Narendra Babu P., "Adaptive Grid-Connected Inverter Control Schemes for Power Quality Enrichment in Microgrid Systems: Past, Present, and Future Perspectives," *Electric Power Systems Research*, vol. 230, 2024. [CrossRef] [Google Scholar] [Publisher Link]

[21] Qinran Hu et al., "Grid-Forming Inverter Enabled Virtual Power Plants with Inertia Support Capability," *IEEE Transactions on Smart Grid*, vol. 13, no. 5, pp. 4134-4143, 2022. [CrossRef] [Google Scholar] [Publisher Link]

[22] Robert H. Lasseter, Zhe Chen, and Dinesh Pattabiraman, "Grid-Forming Inverters: A Critical Asset for the Power Grid," *IEEE Journal of Emerging and Selected Topics in Power Electronics*, vol. 8, no. 2, pp. 925-935, 2020. [CrossRef] [Google Scholar] [Publisher Link]

[23] Levent Yavuz et al., "Transformation of Microgrid to Virtual Power Plant-A Comprehensive Review," *IET Generation, Transmission & Distribution*, vol. 13, no. 11, pp. 1994-2005, 2019. [CrossRef] [Google Scholar] [Publisher Link]